ELSEVIER

Journal of Wind Engineering
and Industrial Aerodynamics 86 (2000) 203–220

JOURNAL OF wind engineering AND industrial aerodynamics

www.elsevier.com/locate/jweia

On the prediction of turbulent flows around full-scale buildings

Paulo J. Oliveira[a,*], Bassam A. Younis[b]

[a]*Departamento de Engenharia Electromecanica Universidade da Beira Interior, Rua Marques D'Avila e Bolama, 6200 Covilha, Portugal*
[b]*Department of Civil Engineering, City University, London EC1V 0HB, UK*

Received 6 October 1999; accepted 16 March 2000

Abstract

Data from tests on a full-scale, single-span high eaves commercial glasshouse are used to quantify the uncertainties associated with the use of computational fluid dynamics to obtain wind load predictions for full-scale structures. It is demonstrated that the widely used assumption of two-dimensional flow field in the mid-span leads to serious overestimation of the suction pressures over the roof and on the leeward wall. It is further shown that the use of a Reynolds-stress closure enables the capture of flow reversal downstream of the windward eaves. In contrast, the industry-standard k–ε model is found to predict no flow separation, contrary to the experimental observation. Finally, guidelines are suggested for suitable mesh distributions and for the efficient sizing of the computational domain relative to the building's dimensions.

Keywords: CFD; Turbulence modelling; Full-scale simulations

1. Introduction

The use of computational fluid dynamics (CFD) in wind engineering involves making a number of assumptions and choices regarding such matters as the size of the computational domain surrounding the structure under consideration, the structure of the atmospheric boundary layer at inlet to this domain, the size and distribution of the computational mesh, the order of accuracy of the discretisation scheme and the type of turbulence model to be used to close the time-averaged equations. Despite the marked increase in the reported use of CFD for wind-load

* Corresponding author.

0167-6105/00/$ - see front matter
PII: S0167-6105(00)00011-8

predictions, the impact of these choices on the quality of the computed results has remained largely unknown, and hence perhaps the limited use to date of CFD in practical design applications. But the case for increased use of CFD is nevertheless quite strong: the standard engineering design codes, the traditional source of wind load data, are known to be somewhat conservative and, moreover, they fail to properly account for the effects of all the relevant flow and geometric parameters [1,2]. Ideally, data from full-scale experiments should be used to further refine the design codes but such data are difficult to obtain, especially when the effects of various parameters are to be studied in isolation. The conduct of such a parametric study is arguably the most appropriate use for computer-based prediction methods but the reliability of the simulations must first be checked, and their sensitivity to the various assumptions be better quantified. This is then the motivation for the present study: to assess how well can full-scale data be predicted by state-of-the-art methods and determine the extent to which these predictions are influenced by the assumptions involved. We take as the benchmark validation data the full-scale measurements of Hoxey and Moran [3] for a single-span, high eaves glasshouse. These measurements have been incorporated into the design code for commercial glasshouses and thus provide a realistic and exacting test for the computations. In what follows, we describe the essentials of the numerical algorithm and the turbulence models used to close the mean-flow equations. We then present and discuss the outcome of over 60 computer runs performed to determine the sensitivity of the solutions to various computational details. The issue of appropriate turbulence modelling for wind-load applications is then considered with particular reference to the adequacy in such flows of the industry-standard k–ε model of turbulence. Conclusions are presented in the final section.

2. The governing equations and their solution

The equations that govern the fluid flow around a full-scale structure are the time-averaged continuity and momentum equations which, for the steady flow of a constant property fluid, are given by

$$\frac{\partial U_i}{\partial x_i} = 0, \tag{1}$$

$$U_j \frac{\partial U_i}{\partial x_j} = \frac{\partial}{\partial x_j}\left(\nu \frac{\partial U_i}{\partial x_j} - \overline{u_i u_j} \right) - \frac{1}{\rho} \frac{\partial p}{\partial x_i}. \tag{2}$$

In the above, U_i is the mean-velocity vector with components U, V and W in the x, y and z directions, respectively, p is the static pressure, ρ is the fluid density and ν is its kinematic viscosity. Repeated indices imply summation.

In the k–ε turbulence closure adopted here, the unknown Reynolds stresses ($\overline{u_i u_j}$) in Eq. (2) are assumed to vary linearly with the local rate of strain, thus

$$-\overline{u_i u_j} = \nu_t \left(\frac{\partial U_i}{\partial x_j} + \frac{\partial U_j}{\partial x_i} \right) - \frac{2}{3} \delta_{ij} k \tag{3}$$

and v_t, the eddy viscosity, is evaluated from:

$$v_t = C_\mu \frac{k^2}{\varepsilon}. \tag{4}$$

The turbulence kinetic energy (k) and its dissipation rate (ε) are obtained from the solution of the transport equations

$$U_j \frac{\partial k}{\partial x_j} = \frac{\partial}{\partial x_j}\left(\frac{v_t}{\sigma_k}\frac{\partial k}{\partial x_j}\right) + P_k - \varepsilon, \tag{5}$$

$$U_j \frac{\partial \varepsilon}{\partial x_j} = \frac{\partial}{\partial x_j}\left(\frac{v_t}{\sigma_\varepsilon}\frac{\partial \varepsilon}{\partial x_j}\right) + C_{\varepsilon_1}\frac{\varepsilon}{k}P_k - C_{\varepsilon_2}\frac{\varepsilon^2}{k}, \tag{6}$$

where P_k is the rate of production of k

$$P_k = -\overline{u_i u_j}\left(\frac{\partial U_i}{\partial x_j} + \frac{\partial U_j}{\partial x_i}\right). \tag{7}$$

The complete model involves a number of coefficients which are here assigned their standard values, viz.,

$$C_\mu = 0.09, \quad C_{\varepsilon 1} = 1.45, \quad C_{\varepsilon 2} = 1.9, \quad \sigma_k = 1.0, \quad \sigma_\varepsilon = 1.3.$$

The model described by Eqs. (3)–(6) forms the basis of the majority of commercial CFD software and is the one most likely to be used in routine engineering calculations. Its shortcomings, however, are many and well-documented: it does not allow for anisotropic diffusivities in three-dimensional strain fields, its representation of the effects of streamline curvature (which are expected to be quite pronounced around the windward eaves) is quite inadequate and its response to the application and removal of streamwise pressure gradients is poor. The rate of production of k seems always to be exaggerated, leading to higher than expected levels of turbulence kinetic energy (and thus higher eddy viscosity). Thus, when used for pitched-roofed buildings, the standard k–ε model either underestimates the extent of the region of the large-scale separation that occurs over the windward roof or fails to predict its occurance altogether. Not surprisingly, therefore, Paterson and Apelt [4] found it necessary to set the velocity just above the front eaves to zero in order to capture the flow separation – clearly an unsatisfactory practice. A number of extensions and enhancements to the standard model have been proposed and tested; none consistently performing better than the standard closure. Hanjalic and Launder [5] made proposals for sensitising the ε production term to irrotational strains but their model is not coordinate invariant and its usefulness in complex flows is therefore limited. Non-linear eddy-viscosity models (e.g. Ref. [6]) have come closest to providing a substitute to the standard model but these are difficult to implement for general non-orthogonal coordinates, and are often badly behaved with regards to numerical stability and convergence.

An altogether different approach for determining the Reynolds stresses, and one which is physically better founded than the eddy-viscosity hypothesis, is to solve differential transport equations in which they are the dependent variables.

Such equations are easily derived from the Navier–Stokes equations and take the form

$$\overbrace{U_k \frac{\partial \overline{u_i u_j}}{\partial x_k}}^{\text{Convection}} = -\overbrace{\left(\overline{u_i u_j}\frac{\partial U_j}{\partial x_k} + \overline{u_j u_k}\frac{\partial U_i}{\partial x_k}\right)}^{\text{Production}\,(P_{ij})} + \overbrace{\frac{\partial}{\partial x_k}\left[\nu\frac{\partial \overline{u_i u_j}}{\partial x_k} + C_s\frac{k}{\varepsilon}\overline{u_k u_l}\frac{\partial \overline{u_i u_j}}{\partial x_l}\right]}^{\text{Diffusion}}$$

$$+\overbrace{\overline{\frac{p'}{\rho}\left(\frac{\partial u_i}{\partial x_j} + \frac{\partial u_j}{\partial x_i}\right)}}^{\text{Redistribution}\,(\phi_{ij})} - \overbrace{2\nu\left(\overline{\frac{\partial u_i}{\partial x_k}\frac{\partial u_j}{\partial x_k}}\right)}^{\text{Dissipation}}, \tag{8}$$

where p' is the fluctuating pressure.

In closing Eq. (8), diffusion by pressure fluctuations was neglected following the usual practice while the triple fluctuating-velocity correlations were modelled with Daly and Harlow's [7] gradient-transport hypothesis, thus

$$-\overline{u_i u_j u_k} = C_s\frac{k}{\varepsilon}\overline{u_k u_l}\frac{\partial \overline{u_i u_j}}{\partial x_l} \tag{9}$$

with the coefficient C_s being assigned the usual value of 0.22.

The 'redistribution' term is so called because it acts to redistribute the turbulence energy among the various components and to reduce the shear stresses. Various alternative proposals for modelling this term may be found in the literature. Most, however, require the use of a 'wall damping' term to represent the effects of a solid boundary in modifying the pressure field in its vicinity. In flows bounded by a single flat wall, the definition of this term does not pose any special difficulty but this is not the case when the flow is influenced by a number of walls, especially when these intersect as in the present application. The definition of an effective normal distance which enters into the 'wall damping' term becomes difficult and models of this kind are thus prone to yield discontinuous solutions. In this work, we adopt the pressure strain model of Speziale, Sarkar and Gatski [8] (hereafter SSG) which is quadratic in the Reynolds stresses and which was shown by Basara and Younis [9] to work well in a number of two-dimensional separated flows without requiring any wall-damping terms. This model is given as

$$\begin{aligned}\phi_{ij} = & -(C_1\varepsilon + C_1^* P_k)b_{ij} + C_2\varepsilon(b_{ik}b_{kj} - \tfrac{1}{3}b_{mn}b_{mn}\delta_{ij}) \\ & + [C_3 - C_3^*(b_{mn}b_{mn})^{1/2}]kS_{ij} + C_4 k(b_{ik}S_{jk} + b_{jk}S_{ik} - \tfrac{2}{3}b_{mn}S_{mn}\delta_{ij}) \\ & + C_5 k(b_{ik}W_{jk} + b_{jk}W_{ik}),\end{aligned} \tag{10}$$

where b_{ij}, S_{ij} and W_{ij} are, respectively, the Reynolds-stress anisotropy, the mean rate of strain and the mean vorticity tensors, defined as

$$b_{ij} = \frac{\overline{u_i u_j}}{2k} - \frac{1}{3}\delta_{ij}, \tag{11}$$

$$S_{ij} = \frac{1}{2}\left(\frac{\partial U_i}{\partial x_j} + \frac{\partial U_j}{\partial x_i}\right), \tag{12}$$

$$W_{ij} = \frac{1}{2}\left(\frac{\partial U_i}{\partial x_j} - \frac{\partial U_j}{\partial x_i}\right). \tag{13}$$

The following values were assigned to this model's coefficients:

$$C_1 = 3.4, \quad C_1^* = 1.80, \quad C_2 = 4.2, \quad C_3 = 0.8,$$

$$C_3^* = 1.30, \quad C_4 = 1.25, \quad C_5 = 0.40.$$

Finally, following Rotta [10], the dissipation of $\overline{u_i u_j}$ was assumed to be isotropic at high turbulence Reynolds number, the

$$2\nu\left(\frac{\partial u_i \partial u_j}{\partial x_k \partial x_k}\right) = \frac{2}{3}\,\delta_{ij}\varepsilon. \tag{14}$$

ε was then obtained from the solution of the equation

$$U_j \frac{\partial \varepsilon}{\partial x_j} = \frac{\partial}{\partial x_j}\left(C_\varepsilon \frac{k}{\varepsilon}\,\overline{u_j u_l}\,\frac{\partial \varepsilon}{\partial x_l}\right) + C_{\varepsilon_1}\frac{\varepsilon}{k}\,P_k - C_{\varepsilon_2}\frac{\varepsilon^2}{k}. \tag{15}$$

The coefficients of this equation were assigned the values recommended by Speziale et al. [8]

$$(C_\varepsilon, C_{\varepsilon 1}, C_{\varepsilon 2}) = (0.183, 1.44, 1.83).$$

The solution of the above equations was achieved, iteratively, using a finite-volume method based on that of Peric [11]. The method utilises general, non-orthogonal, coordinates and stores all the dependent variables at the cells centres. In performing three-dimensional simulations, the computer time and memory are often wasted by the redundant placement of computational meshes within the buildings themselves. This is avoided in the present study by the use of a special 'indirect addressing' technique, developed by Oliveira [12], which ensures that all the grid nodes used lie within the flow region and are thus active. Implementation of the Reynolds-stress closure is fairly straightforward: the gradients of the Reynolds stresses are introduced as sources to the momentum equations; the cell-face values of these stresses are evaluated by linear interpolation of the nodal values and zero-flux wall boundary conditions are assumed for all the Reynolds stresses. The gradients of mean velocity in the direction normal to the wall were evaluated (at the grid nodes closest to the wall) from direct differentiation of the log-law; a practice which is generally found to enhance the coupling between the solutions of the mean-flow and turbulence fields.

The remaining boundary conditions were as follows. At the inlet to the computation domain, the mean-flow and turbulence profiles were obtained by simulating the atmospheric boundary layer using a standard boundary-layer code and the SSG model. The resulting equilibrium boundary layer was self-sustaining with a thickness of 300 m and a ridge-height velocity of 9.02 m/s. A ground-roughness parameter (y_0) of 10 mm was assumed in these simulations (after Hoxey and Richards [13]). The

predicted mean streamwise velocity agreed very well with the log-law correlation for rough surfaces. At the outlet from the computational domain, i.e., at $x = L_2 + S$, the axial gradients of all dependent variables were set equal to zero implying a fully developed flow at exit. The top of the computational domain (i.e., at $y = Y$) was assumed to be a plane of symmetry and thus the vertical gradients of all the dependent variables were set equal to zero except for the shear stresses which were themselves set equal to zero. Close to the wall, turbulence dissipation rate was set equal to the local turbulence energy production and the momentum fluxes that form the boundary conditions for the velocity components parallel to the wall were deduced from the logarithmic law of the wall.

3. Presentation and discussion of results

A schematic representation of the glasshouse tested by Hoxey and Moran [3] is given in Fig. 1 which also shows the coordinate system used and defines the principal dimensions. The glasshouse (referred to a G08 in the original study) is 22.6 m long (L) and has a span (S) of 7.0 m. The eaves are at a height (H) of 4.15 m and the ridge height (H') is 5.86 m. The roof pitch is 27°.

3.1. Influence of grid size and distribution

A summary of the meshes used in computations carried out under this heading is presented in Table 1. NX, NY and NZ there refer to the number of nodes in the x, y and z directions, respectively. NC refers to the total number of control volumes located within the flow domain and $\delta x_{\min}$ and $\delta y_{\min}$ refer to the size (normalised with H) of the smallest grid spacings in the x and y directions respectively. The three-dimensional grids were formed by translating their two-dimensional counterparts along the lateral (z) direction.

The results for the two-dimensional simulations with various grids are presented in Fig. 2. Several interesting features are immediately apparent. The pressure

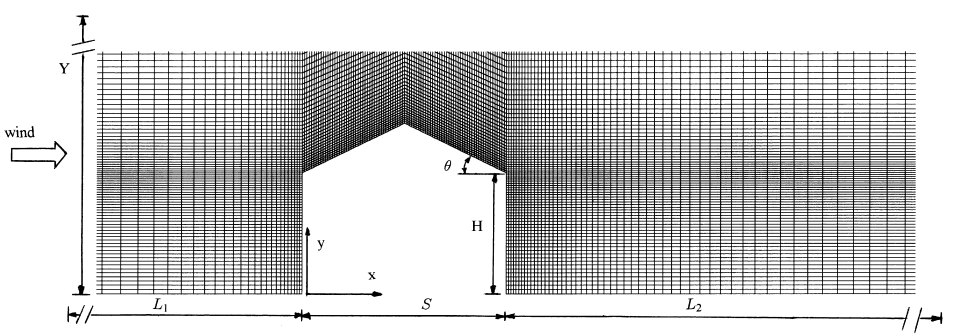

Fig. 1. Computational domain and example of a fine 2-D mesh.

Table 1
Summary of computational grids used

Mesh	NX	NY	2-D			3-D	
			NC	$\delta x_{\min}$	$\delta y_{\min}$	NZ	NC
Coarse	45	25	925	0.084	0.100	30	30750
Medium-1	45	50	1850	0.084	0.019	30	61500
Medium-2	90	50	3700	0.042	0.019	–	–
Medium-3	65	50	2450	0.019	0.019	30	85500
Fine-1	225	80	17240	0.044	0.050	–	–
Fine-2	225	100	18980	0.019	0.016	–	–

distribution over the windward wall appears to be insensitive to the choice of grid: increasing the number of grid nodes by a factor of 20 yields hardly a discernable change in C_p. The predicted pressures on the leeward side are somewhat more sensitive to the grid size though all the grids tested seem to produce a very uniform distribution across the entire wall. A very different behaviour is observed for the pressure distribution on the roof where the pressure distributions are far from uniform and where, even after discounting the coarse-grid results, quite substantial differences are apparent for the various grids. The pressure peak on the windward roof close to the ridge, a feature of many CFD studies, is clearly seen to be a grid-induced phenomenon which disappears with further refinement. Note that on the leeward wall, increasing the number of nodes from 17 240 (in fine-1) to 18 980 (in fine-2) actually worsens the prediction of the pressure recovery over that side. The reason for this unexpected result is because grid 'fine-1' is formed from uniformly sized meshes and does not therefore provide adequate resolution for the near-wall regions where large variations in velocity and pressure occur. This is a classic case where the numerical errors introduced by an inappropriate grid distribution produce, quite spuriously, closer agreement with the data! Note finally that irrespective of the grid used, all the predictions are in very poor agreement with the data, even after allowing for the estimated 7% error in the measurements.

Checks on the sensitivity of three-dimensional simulations to grid effects are much harder to perform as it becomes quite easy to exceed the memory available on typical engineering workstations. For this reason, we confine our study here to the examination of the three-dimensional grids obtained by translating in the spanwise direction the 'medium' grids that have produced sensible results for the two-dimensional tests. The predicted and measured pressure coefficients are compared in Fig. 3. The pressures on the windward and leeward walls once again appear to be insensitive to the choice of grid density. Indeed, it would appear that the principal differences are due to a shift in the absolute values of these coefficients, with little change in the profile shapes. Note the reduction in the pressure peak near the ridge with grid refinement – a feature similar to that observed in the two-dimensional case.

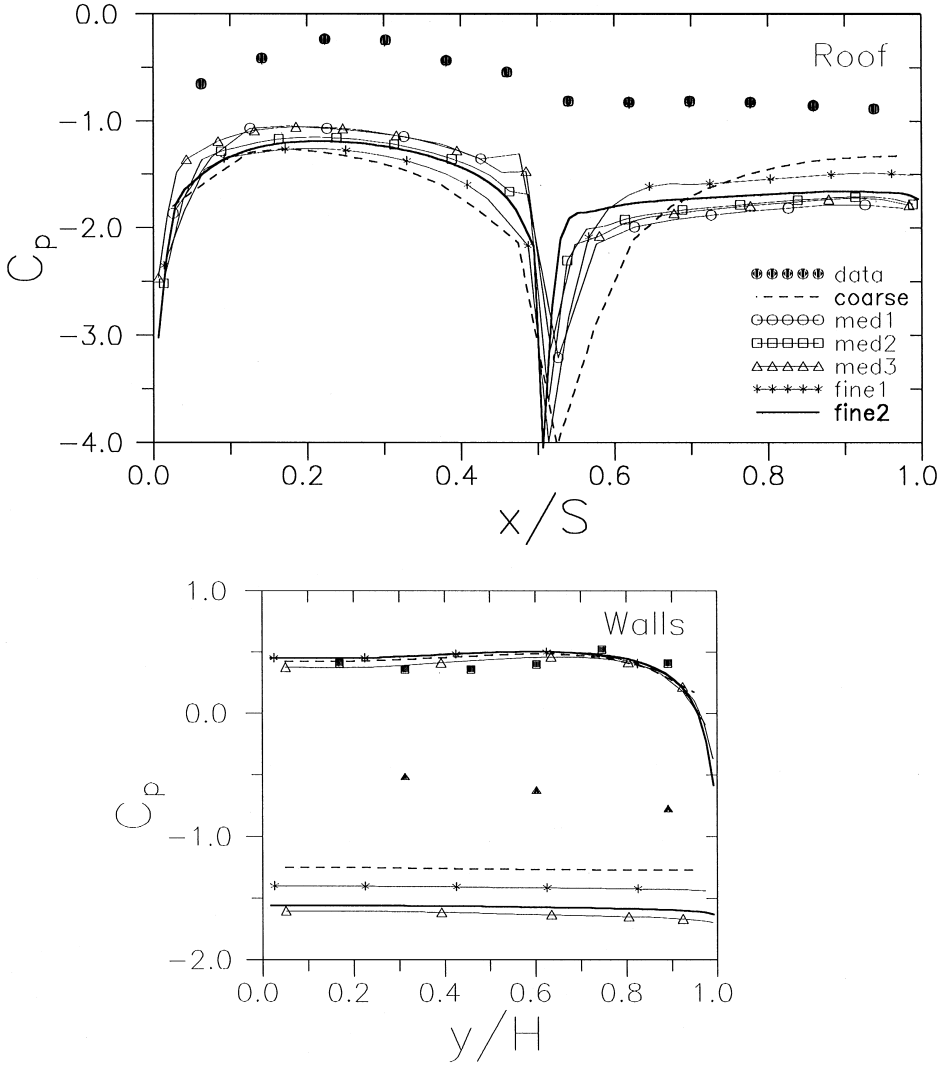

Fig. 2. Mesh refinement in the 2-D simulations.

3.2. *Influence of domain size*

We determine the influence on the predictions of the choice of distance from the inlet plane to the glasshouse (L_1 in Fig. 1) and of the distance (Y) above the ground where the boundary conditions are applied. Some guidance on the size of the computational domain can already be found in the programme of computations and field experiments conducted by Hoxey and Richards [13] on a low-rise, rural-type building. They reported that the pressure field was affected by the presence of the

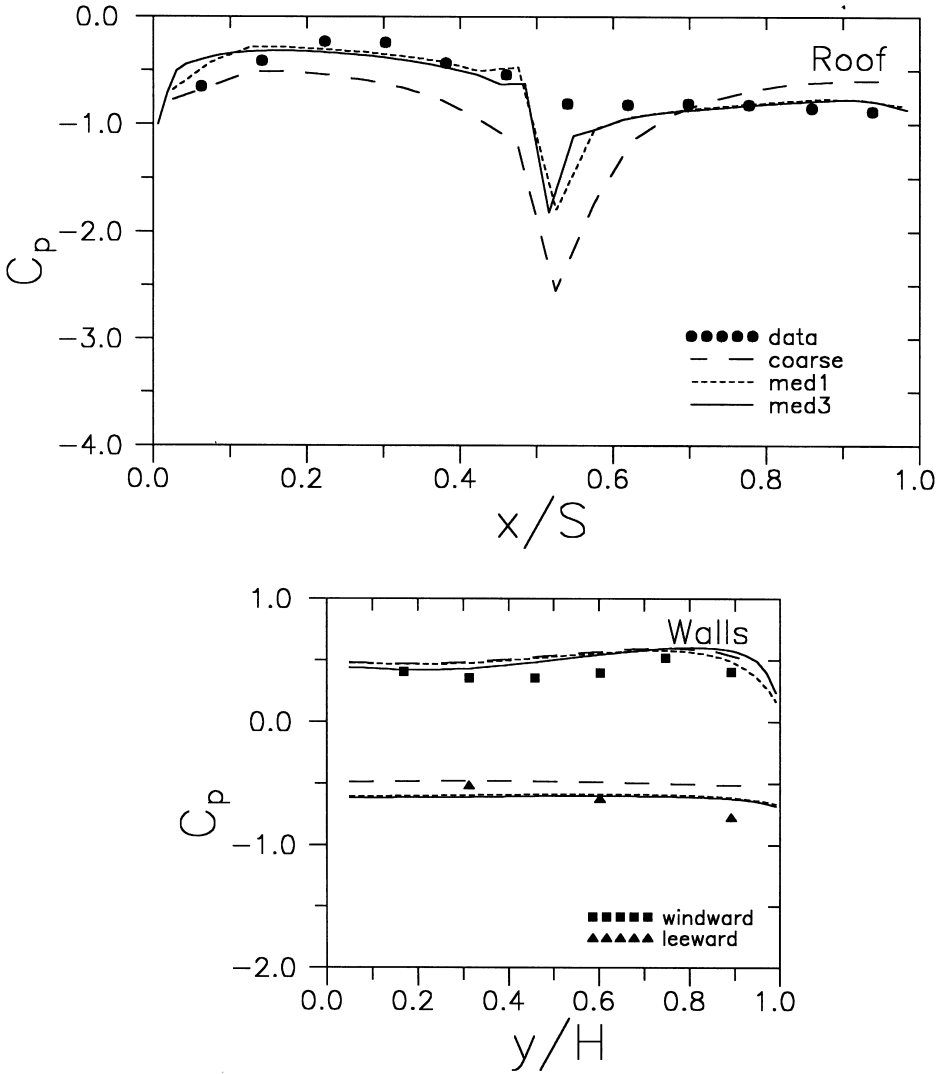

Fig. 3. Mesh refinement in the 3-D simulations.

building up to a distance of 4–5 building heights upstream of it and to a distance of 4 heights on either side. Based on these findings, we take L_1 and Y as 21 and 20.75 m, respectively, to obtain $L_1/S = 3$ and $Y/H = 5$.

With the entry length L_1 held constant at 21 m, the effect of increasing Y can be seen from Fig. 4. A small domain causes severe blockage effect, leading to increased flow speed and reduced pressure on the roof and the leeward wall. A domain depth of about 10 heights appears to be sufficient to produce results that are essentially independent of the depth of the computational domain.

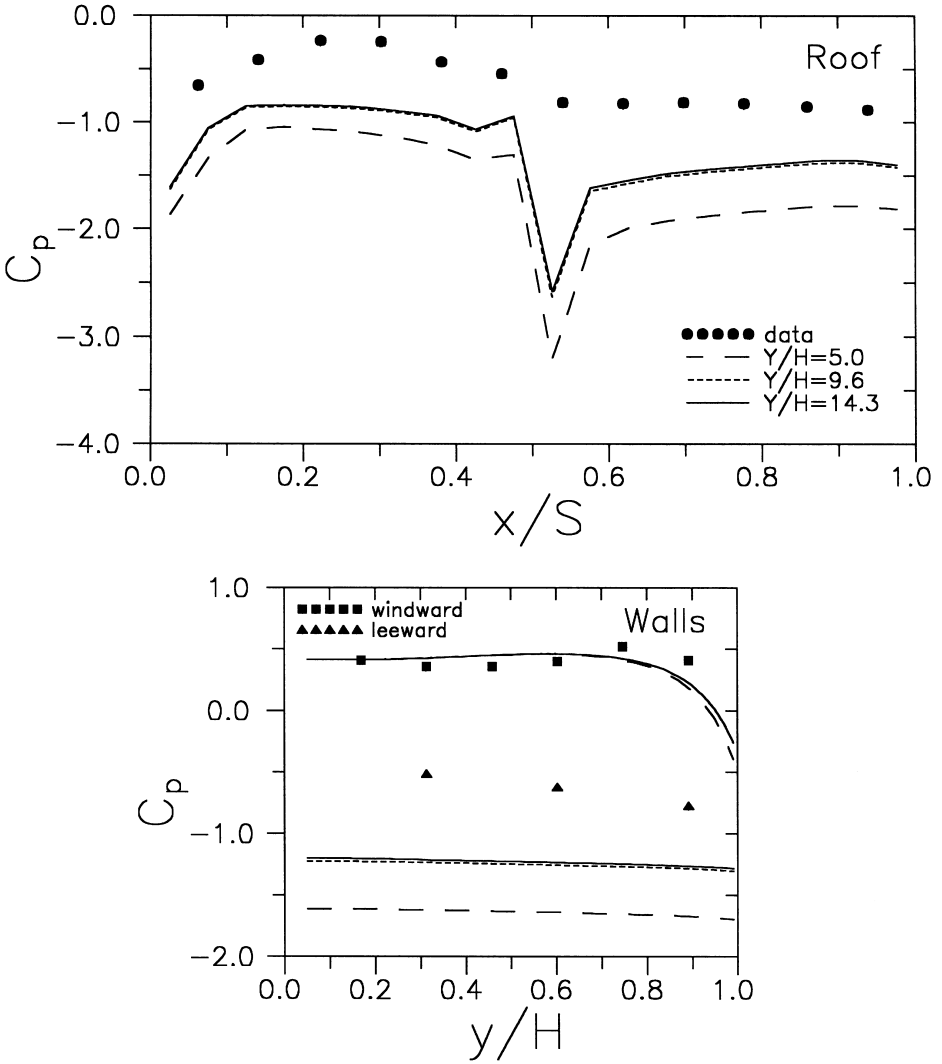

Fig. 4. Effect of increasing domain height (Y) on pressure coefficients. (2-D calculation, upstream length, $L_1 = 3S$).

The effect of increasing L_1 (while keeping Y constant at $Y/H = 10.8$) is shown in Fig. 5. The result is similar to Fig. 4, with a very pronounced reduction of suction around the building. A value of L_1/H of around 15 seems to be sufficient. It thus appear that the blockage effect imposed by a building on an approaching wind flow is very important in 2-D simulations, requiring a domain higher than $10H$ and an upstream developing length longer than $15H$ in order to obtain predictions that are independent of the assumed computational domain size.

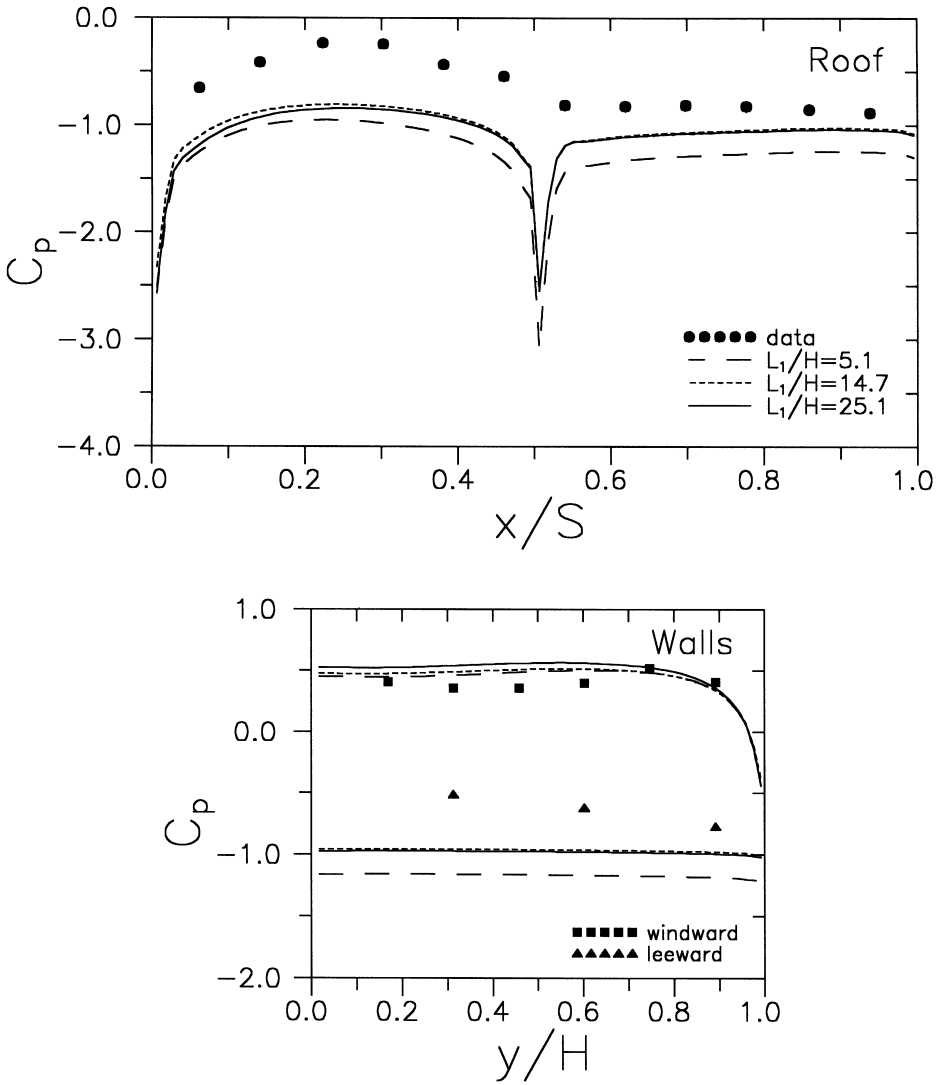

Fig. 5. Effect of increasing upstream length (L_1) on pressure coefficients. (2-D fine-2 mesh, $Y/H = 10.8$).

The situation for the three-dimensional simulations is markedly different, as can be inferred from Fig. 6 where the predicted C_p variation on the roof and side walls is shown for $Y/H = 5$ and 9.6. The results show very little sensitivity to the domain depth. An explanation for such different behaviour between the 2-D and 3-D simulations resides in the higher blockage ratio in the 2-D case (= 20%) compared to the 3-D case (about 7%). In the latter case, air is free to flow around the ends of the building and hence the lower suction pressures on the roof. Fig. 6 shows that L_1/S

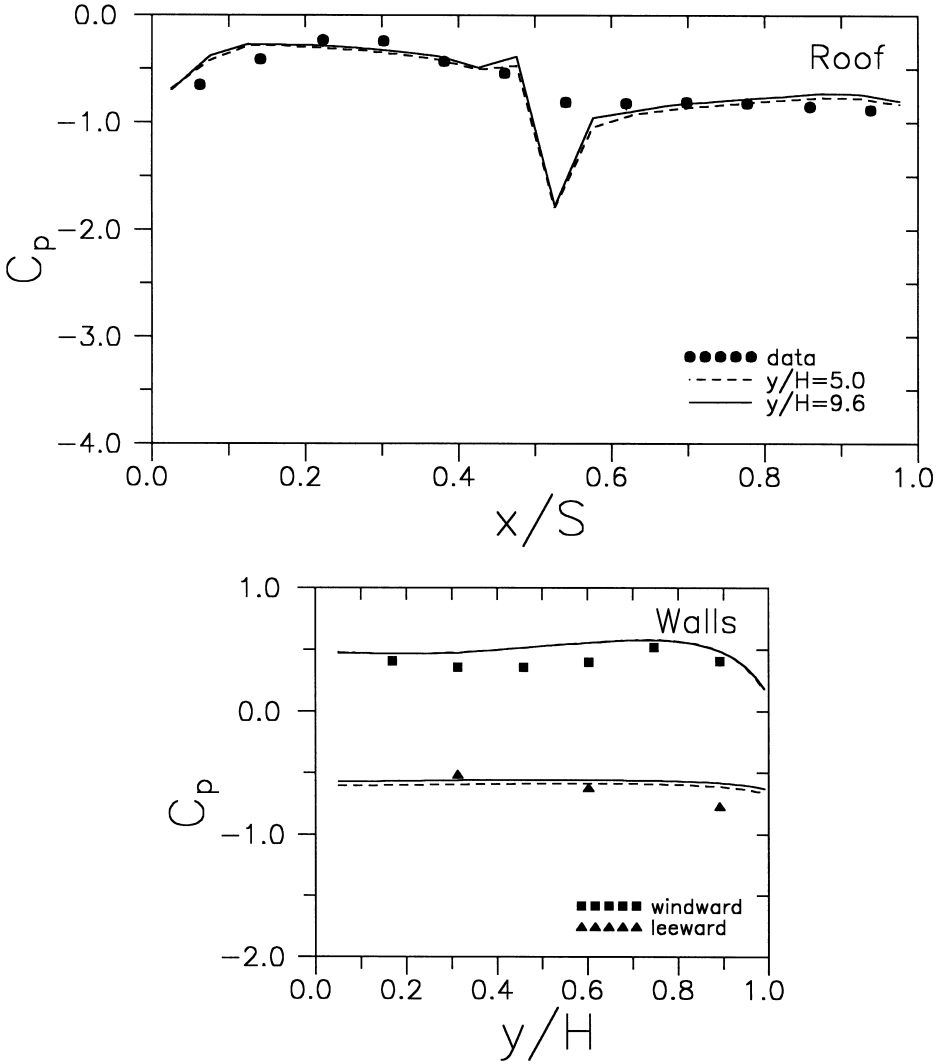

Fig. 6. Effect of increasing domain height (Y) on pressure coefficients for 3-D calculations.

of 3 and Y/H of 5 give adequate results, and so these values will be used in the remaining 3-D simulations.

3.3. *Influence of assumed dimensionality*

Fig. 7 compares the best results to emerge from the two- and three-dimensional simulations. Whereas the results of the 3-D simulation are quite close to the experimental full-scale measurements, the 2-D simulation predicts too much negative

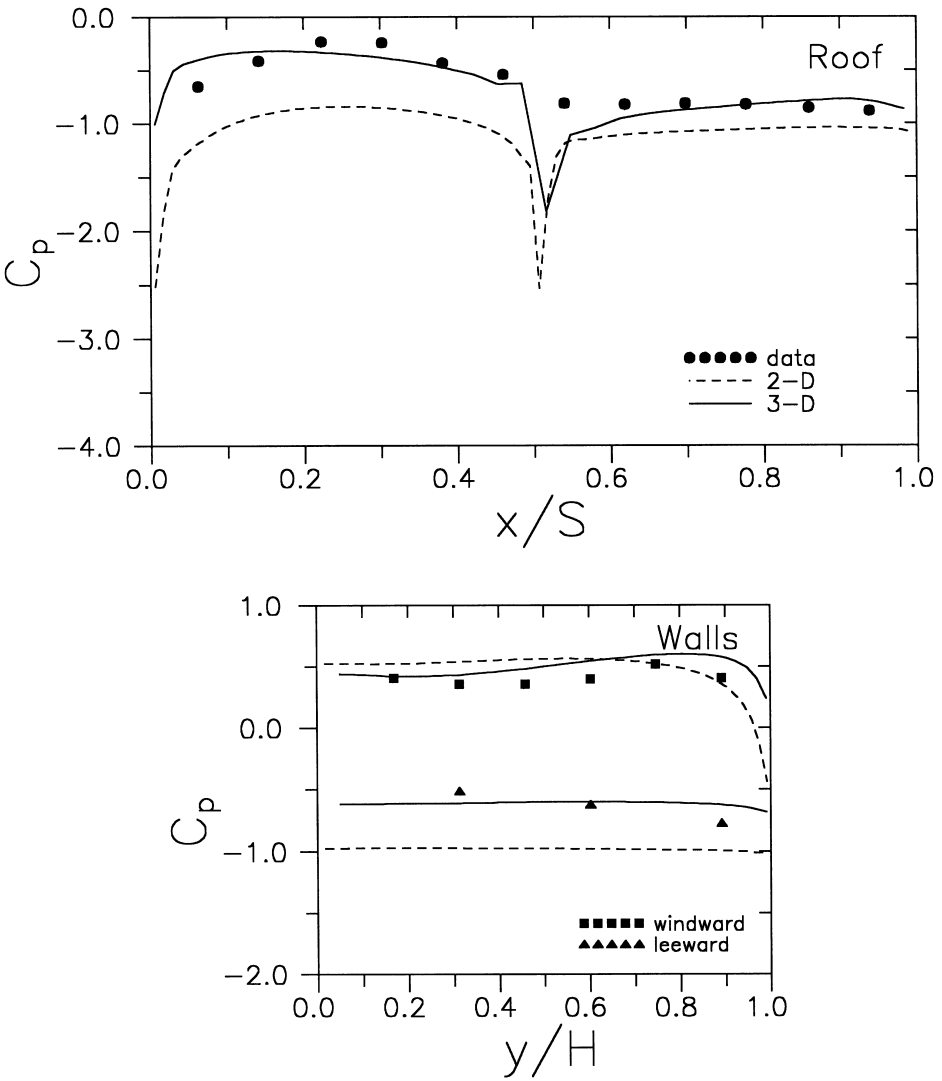

Fig. 7. Comparison of measured pressure coefficients with predictions of the 2-D and 3-D simulations.

pressures on the roof and on the leeward wall, bearing in mind that these results are independent of the size of the computational domain. Blame for such inadequate results cannot be placed on the choice of turbulence model (see next section), but must in part be due to the large roof-pitch angle of building G08, which produces excessive upward deflection of the incident flow. There is another contributor, namely the end effects which cause strong swirling motions. These are clearly seen in Fig. 8, where velocity vector plots are shown at several cross-stream planes

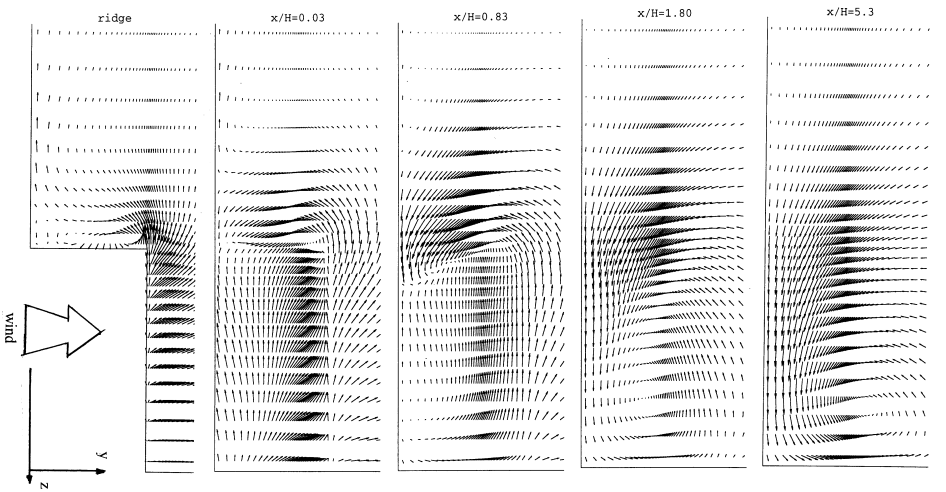

Fig. 8. Predicted velocity field in planes perpendicular to the main wind direction: (a) plane at ridge line ($x/S = 0.5$); (b) first plane downstream from leeward wall ($x/S = 1.02$); (c) sixth plane downstream from leeward wall ($x/S = 1.49$); (d) eighth plane downstream from leeward wall ($x/S = 2.07$); and (e) eleventh plane downstream from leeward wall ($x/S = 4.2$) (The x/H at the side of the figures is measured from the leeward wall.). (See figure from left side.)

downstream from the building ridge plane. Small counter-clockwise rotating vortices form at the end ridge-corners ($z = -L/2$, $y = H'$) and develop quickly as the flow progresses downstream into big vortices, which bring the flow from outside into the main recirculation zone behind the building. Velocities in the cross-wind planes attain up to 35% of the main mean wind velocity. The net effect is to decrease the suction on the leeward wall and also over the roof.

3.4. *Influence of turbulence model*

We consider first the sensitivity of the two-dimensional simulations to the choice of turbulence model. Fig. 9 compares the k–ε and Reynolds-stress model results for the pressure distribution. There is considerable difference between the two models predictions, especially in the region between the windward eaves and the ridge where the Reynolds-stress model predicts a reduced pressure distribution typical to that associated with a locally separated flow. The presence of a region of flow reversal over the windward roof is confirmed from the plots of mean-flow streamlines presented in Fig. 10. That the standard k–ε model does not capture the expected flow separation over the windward eaves has been observed by Hoxey et al. [14] and by Hoxey and Richards [13]. Various ad hoc corrections to the basic model to improve its performance in this region have been proposed in the literature; none with any real promise of generality. On the other hand, the Reynolds-stress closure is clearly able to predict flow separation at the windward eaves without recourse to any modification. It does

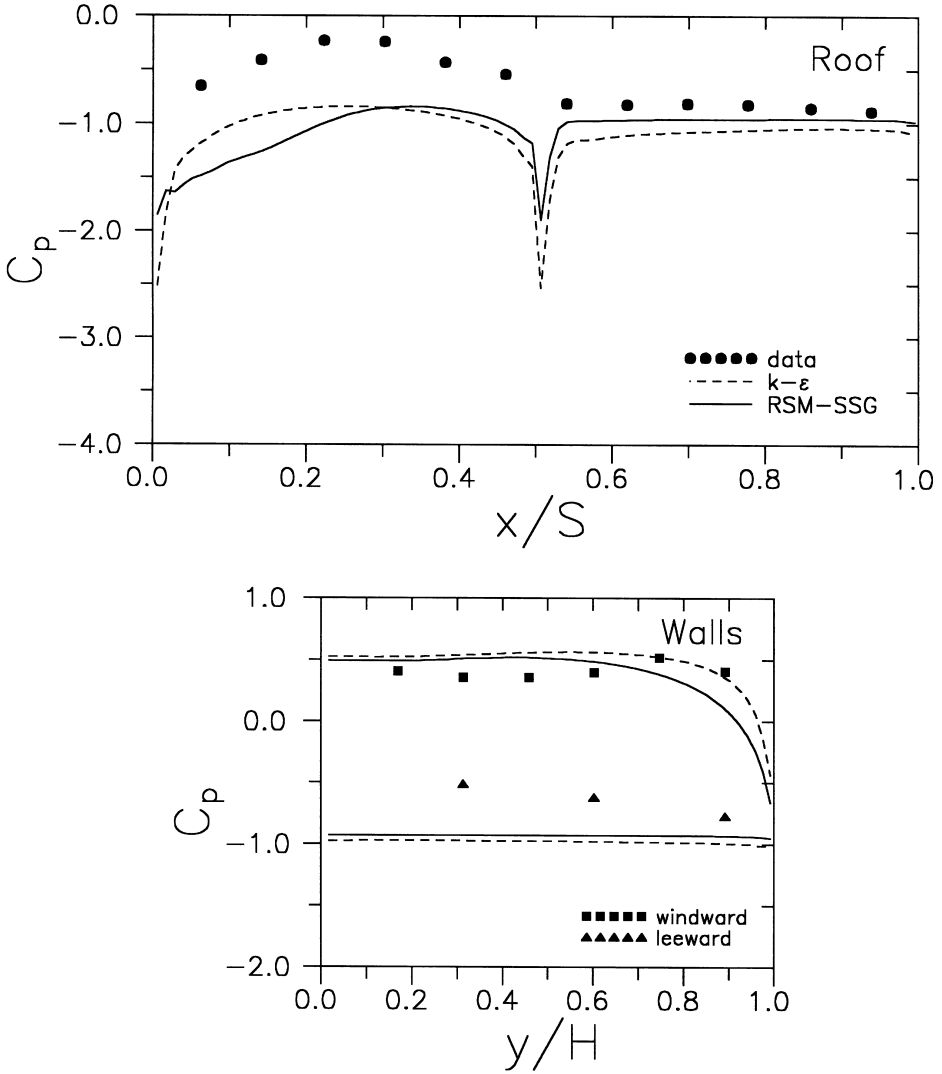

Fig. 9. Pressure distribution predicted with the two turbulence models (2-D simulations).

so primarily by returning reduced levels of turbulence kinetic energy which, in turn, is a consequence of allowing for the production of k to become negative, where appropriate.

Turning next to the three-dimensional simulations, the differences here between the k–ε and Reynolds-stress model results are not as substantial as before. This can be seen from Fig. 11 where the pressure distributions on the roof and walls are compared. This is partly due to the absence in these simulations of a separated flow region above the roof, consistent with the reduction in the blockage effect noted

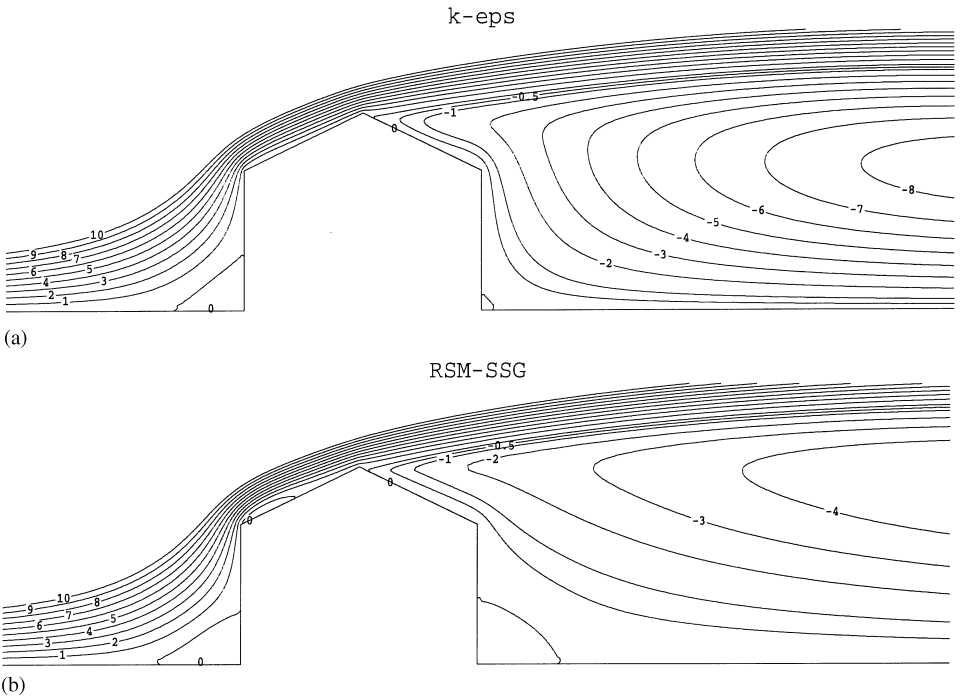

Fig. 10. Detail of the streamlines around the building to show possible local separation: (a) 2-D predictions with the k–ε model; and (b) 2-D predictions with the RSM-SSG model.

earlier. A quantitative measure of the difference between the two models is provided by the integration of the pressure distribution to obtain a single, averaged, value appropriate to a section through the mid-length plane. The Reynolds-stress model obtains this quantity as -0.596 while the k–ε model value is -0.686: an overestimation of the roof suction by about 15%.

4. Conclusions

Simulations of the wind flow around a full-scale low-rise building have been performed to determine the sensitivity of the solutions to various approximations and assumptions inherent to the numerical solution of the governing equations. It was found that performing these computations with the assumption of two-dimensional flow along a mid-length plane leads to a serious overestimation of the roof suction loads. Contributions to this outcome arise from the well-known blockage effect as well as from the presence, in the three-dimensional case only, of a strong streamwise vortex which substantially alters the patterns of flow around the building. The value of two-dimensional simulations is therefore confined to the guidance they provide for constructing grids suitable for three-dimensional

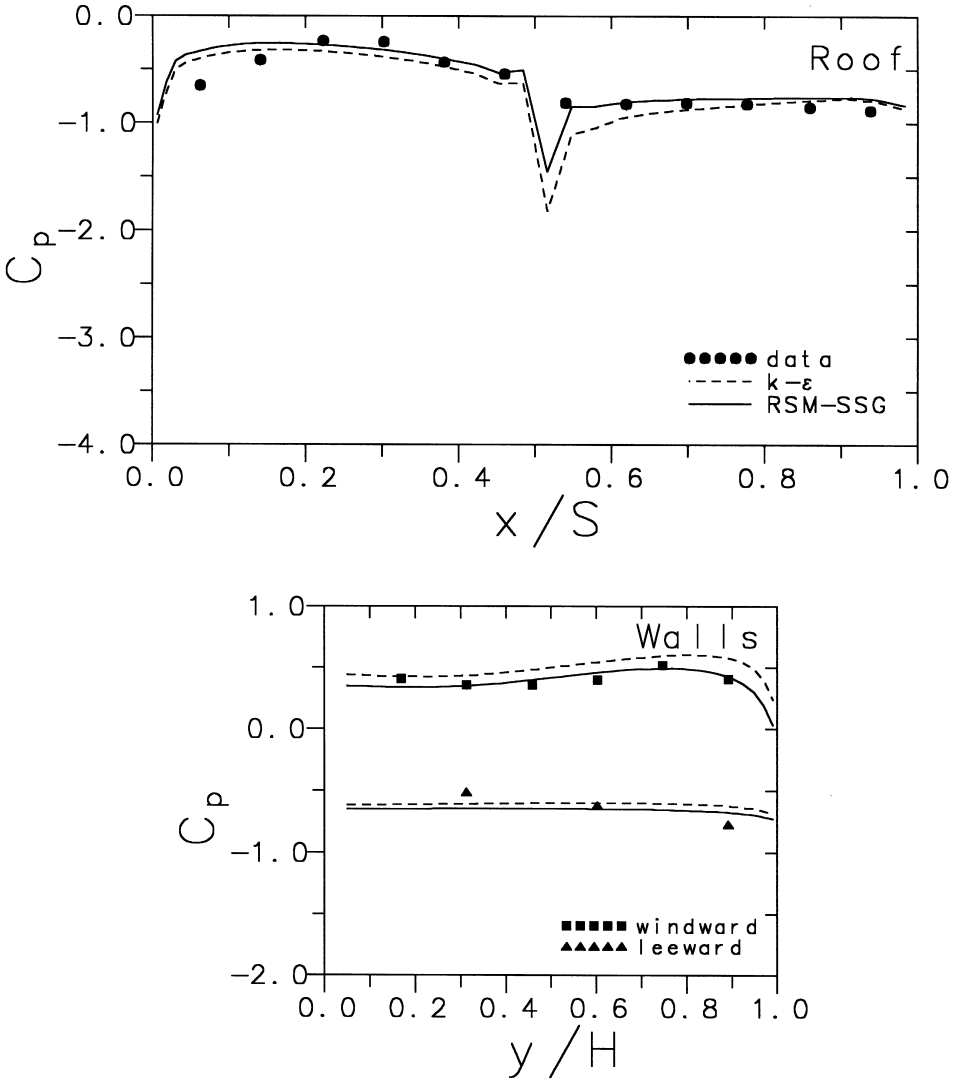

Fig. 11. Pressure distribution predicted with the two turbulence models (3-D simulations).

simulations. The influence of the domain size, while substantial in the two-dimensional simulations, was found to be quite moderate in the three-dimensional simulations provided that the building is placed at a distance of at least $3S$ (around $5H$) from entry to the computational domain and the external boundary conditions applied at a distance of at least $5H$ from the sides and $4H$ from the roof of the building. The use of a Reynolds-stress closure enables the prediction of flow separation on the windward side of the roof, with consequent changes in the wall static-pressure distribution. No flow separation is obtained with the k–ε model, consistent with previous findings.

Acknowledgements

We gratefully acknowledge the financial support of the EPSRC under grant GR/H/45643 and of the STRIDE Commission (EC), FEDER and JNICT (Portugal) under grant STRDE/C/CEG/719/92. P.J. Oliveira wishes also to express his gratitude to Fundacao para a Ciencia e a Tecnologia (FCT, Portugal) for funding under grant FMRH/BSAB/68/98. Thanks are due to Dr. Roger Hoxey (Silsoe Research Institute, UK) for providing us with tabulated data. Authors' names appear alphabetically.

References

[1] R.P. Hoxey, A.P. Robertson, Pressure coefficients for low-rise building envelopes derived from full-scale experiments, J. Wind Eng. Ind. Aerodyn. 53 (1994) 283–297.
[2] R.P. Hoxey, P. Moran, A full-scale study of the geometric parameters that influence wind loads on low rise buildings, J. Wind Eng. Ind. Aerodyn. 13 (1983) 277–288.
[3] R.P. Hoxey, P. Moran, Full scale wind pressure and load experiments – single-span 7.0×22.6 m glasshouse, Division Note DN. 1605, AFRC Engineering Research, Silsoe, February 1991.
[4] D.A. Paterson, C.J. Apelt, Simulation of wind flow around three-dimensional buildings, Building Environ. 24 (1989) 39–50.
[5] K. Hanjalic, B.E. Launder, Sensitizing the dissipation equation to irrotational strains, ASME J. Fluid Eng. 102 (1980) 609–638.
[6] C.G. Speziale, On nonlinear K–l and K–ε models of turbulence, J. Fluid Mech. 178 (1987) 459–475.
[7] B. Daly, F. Harlow, Transport equations in turbulence, Phys. Fluids 13 (11) (1970) 2634–2649.
[8] C.G. Speziale, S. Sarkar, T.B. Gatski, Modelling the pressure-strain correlation of turbulence: an invariant dynamical systems approach, J. Fluid Mech. 227 (1991) 245–272.
[9] B. Basara, B.A. Younis, Predictions of turbulent flows in dredged trenches, J. Hydraulic Res. 33 (6) (1995) 813–824.
[10] J.C. Rotta, Statistische theorie nichthomogener turbulenz, Z. Phys. 125 (1951) 547–572.
[11] M. Peric, A finite volume method for the prediction of three-dimensional fluid flow in complex geometries, Ph.D. Thesis, Imperial College, University of London, 1985.
[12] P.J. Oliveira, Computer modelling of multidimensional multiphase flow and application to T-Junctions, Ph.D. Thesis, Imperial College, University of London, 1992.
[13] R.P. Hoxey, P.J. Richards, Flow pattern and pressure field around a full-scale building, J. Wind Eng. Ind. Aerodyn. 50 (1993) 203–212.
[14] R.P. Hoxey, A.P. Robertson, B. Basara, B.A. Younis, Geometric parameters that affect wind loads on low rise buildings: full-scale and CFD experiments, J. Wind Eng. Ind. Aerodyn. 50 (1993) 243–252.